technologies

MDPI

Article

Post-Construction Settlement Prediction of Deep Lacustrine-Fluvial Soft Ground Improved by Vacuum Wellpoint Dewatering and Dynamic Compaction: An Engineering Case Study

Wenkai Yang [1], Jie Ouyang [2,*], Zhu Wang [1], Ye Xie [1], Jiale Meng [2] and Cong Zhang [2,*]

[1] Hunan Province Navigation Engineering Co., Ltd., Changsha 410018, China; yangwk19881212@icloud.com (W.Y.); saiwang2013@gmail.com (Z.W.); 13142039988@163.com (Y.X.)
[2] Central South University of Forestry and Technology, Changsha 410004, China; 15560912673@163.com
* Correspondence: 20251200550@csuft.edu.cn (J.O.); zc8023cl@163.com (C.Z.)

Abstract

Deep lacustrine–fluvial soft ground at the Songyanghu Terminal (Phase III), Yueyang Chenglingji Port, was treated using vacuum wellpoint dewatering combined with dynamic compaction. A two-dimensional coupled solid-mechanics-Darcy model in coupled COMSOL Multiphysics 6.3 model was used to examine deformation and excess pore-water-pressure response, while an archived 360-day settlement series was used to evaluate three empirical prediction methods. The field dataset contains 12 settlement observations at a constant 30-day interval from Day 30 to Day 360. The numerical outputs indicate surface settlement approaching approximately 100 mm by Day 100; at Day 10, localised excess pore-water pressure remained at roughly 100 kPa near the mid-depth drainage zone, while most of the model domain was substantially lower. To avoid treating the same observations as both fitting and validation data, the Asaoka, hyperbolic and exponential methods were recalibrated using data ending at Days 180, 240 and 300 and then evaluated against the subsequent withheld observations. Across these three windows, the mean RMSE values were 0.02, 0.59 and 0.19 mm for the Asaoka, hyperbolic and exponential methods, respectively. The Day-360 measurement of 108.84 mm is therefore used as a reference observation rather than as a proven final settlement. For this single site and dataset, the Asaoka method produced the lowest numerical withheld-data errors; however, the differences between the Asaoka and exponential predictions are smaller than the stated ±1 mm levelling accuracy and therefore do not establish statistically or physically significant superiority. Broader applicability requires validation at additional sites and with independent monitoring datasets. These results provide a case-specific basis for post-construction settlement assessment of similarly treated soft ground.

Keywords: soft soil foundation; vacuum wellpoint dewatering; dynamic compaction; combined reinforcement; post-construction settlement; out-of-sample validation

Academic Editor: Luis Fernando Alarcón

Received: 9 August 2026
Revised: 10 September 2026
Accepted: 15 September 2026
Published: 18 September 2026

1. Introduction

Soft soil strata are widely distributed in riverine, coastal and lakeside areas and commonly exhibit high water content, high compressibility and low permeability [1–3]. Under construction and operational loads, these deposits may undergo substantial total and differential settlement, affecting long-term serviceability [4]. Common treatment methods include preloading [5,6], vacuum preloading [7,8], mixing piles [9,10], dynamic compaction [11,12] and combined techniques [13,14]. Vacuum wellpoint dewatering can lower the groundwater level and improve drainage conditions before and during compaction; however, deep soft deposits may still undergo long-term post-construction deformation. Reliable settlement prediction therefore remains important for maintenance planning and deformation control.

Settlement prediction approaches for soft ground include analytical solutions [15], numerical simulations [16,17] and monitoring-data-based fitting or prediction methods [18–20]. Gao Yanxi et al. [20] improved the exponential curve method by considering the starting time and instantaneous settlement; Li Bo et al. [21] proposed a staged superposition model for deep soft ground; Liu Zhi et al. [22] compared several conventional fitting methods; Chen Kai et al. [23] developed a practical method covering the full consolidation process; and Han Shanpeng et al. [24] showed that prediction accuracy can depend strongly on the fitting period and monitoring dataset. More recent studies have examined monitoring-based parameter inversion [25], staged-loading prediction [26], sparse-data regression Kriging [27] and machine-learning prediction under rolling dynamic compaction [28,29]. Collectively, these studies demonstrate that prediction performance is sensitive to loading history, soil heterogeneity, data density and the selected calibration period.

Despite this progress, the literature has not resolved which conventional monitoring-based method performs most reliably for deep lacustrine–fluvial soft ground treated by vacuum wellpoint dewatering combined with dynamic compaction. The contribution of this study is not a new prediction equation; rather, it combines a coupled numerical description of the treated ground with a case-specific, out-of-sample comparison of the Asaoka, hyperbolic and exponential methods using withheld monitoring periods. This design reduces the risk of overstating predictive accuracy when the same observations are used for both calibration and evaluation.

Accordingly, the specific objectives of this study are:

(1) To quantify the temporal response of ground settlement and excess pore-water pressure using the coupled COMSOL Multiphysics 6.3 model;
(2) To characterise the available 360-day post-construction settlement series consisting of 12 observations at 30-day intervals;
(3) To evaluate the out-of-sample performance of the Asaoka, hyperbolic and exponential methods using multiple calibration windows and withheld observations.

2. Project Overview and Integrated Reinforcement Plan

2.1. Project Overview and Geological Characteristics

Phase III of the Yueyang Chenglingji Port Area project is situated in the Songyanghu Subdistrict, Yunxi District, Yueyang City. Located at the strategic junction of the middle reaches of the Yangtze River and the Dongting Lake Eco-Economic Zone, it forms an integral part of the Dongting Lake Eco-Economic Zone. The specific location of the project is at approximately 225.0 km along the middle reaches of the Yangtze River; it is situated approximately 5.4 km upstream from the old Chenglingji Port and approximately 7.0 km downstream from the Jingyue Yangtze River Bridge. The total area requiring ground improvement works is approximately 200,000 square metres, covering five open-air storage yards, two modern warehousing facilities, and associated living support areas and road networks. As the project site is situated on a typical alluvial plain along the river, characterised by a high water table and extensive layers of soft soil of considerable thickness, the quality of the ground improvement works directly affects the safety and stability of the port area's subsequent operations. The layout plan of the wharf is shown in Figure 1.

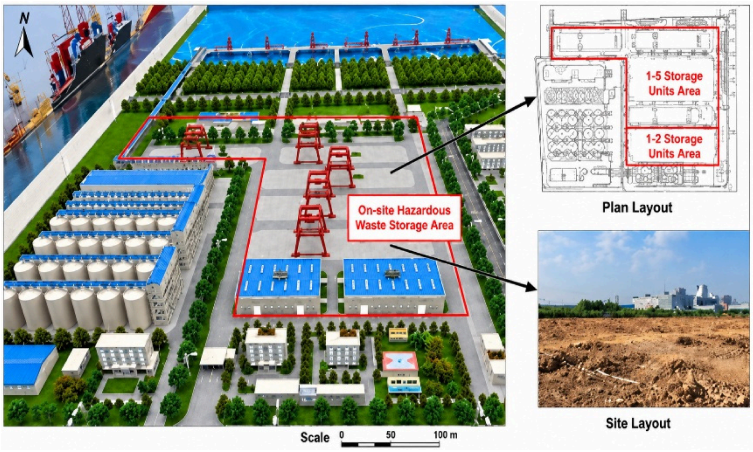

Figure 1. Project layout of Songyanghu Terminal (Phase III).

The site is situated on a typical alluvial plain in the middle reaches of the Yangtze River. This type of ground is characterised by high water content, high compressibility and low permeability, and the groundwater table remains at a high level over the long term. The geological structure of the site exhibits typical dual-layer sedimentary characteristics, with the overlying strata displaying complex physical and mechanical properties and varying degrees of hardness. Specific stratigraphic parameters and ground condition indicators are detailed in the Tables 1 and 2.

Table 1. Stratigraphic parameters.

Stratum Name	Elevation (m)	Natural Density ρ (g/cm^3)	Porosity φ	Compression Modulus E_s (MPa)	Poisson's Ratio	Cohesion c (kPa)	Internal Friction Angle φ (°)	Hydraulic Conductivity K (m/s)
Plain fill	−2.38	2.03	0.457	3.5	0.3	11.0	8.0	1×10^{-6}
2-1 Silty clay	−4.69	1.86	0.465	5.0	0.28	18.5	9.0	1×10^{-8}
Mucky clay	−7.65	1.67	0.585	3.0	0.35	7.5	5.0	2.25×10^{-9}
Clay	−9.17	1.9	0.480	4.5	0.25	16.0	8.5	4.36×10^{-7}
Mucky silty clay	−12.99	1.81	0.538	3.0	0.32	7.5	5.0	2.15×10^{-8}
Silt and sand intercalated with silty clay	−15.73	1.9	0.428	9.0	0.28	18.5	16.5	1.12×10^{-6}
3-1 Silty clay	−18.32	1.91	0.485	8.5	0.26	28	11	1.25×10^{-8}

Note: The stratigraphic parameter set in Table 1 was adopted from the project investigation data used to establish the numerical model.

Table 2. Foundation control specification.

Functional Zone	Standard Value of Foundation Bearing Capacity (kPa)	Resilient Modulus (MPa)	Post-Construction Settlement (cm)
Production area roads	≥100	≥60	≤30 [30]
Warehouses No. 1 and No. 2	≥120	≥60	≤30
Storage yard	≥100	≥60	≤40 [30]
Living area roads	≥80	≥35	≤40

2.2. Combined Reinforcement Scheme

Taking into account the project schedule and cost-effectiveness, relying solely on the traditional preloading method is too time-consuming, whilst the direct application of dynamic compaction in saturated clay is highly likely to cause the build-up of pore-water pressure, leading to the 'rubber soil' phenomenon, which makes it difficult to guarantee the quality of the reinforcement. To this end, a technical solution combining vacuum wellpoint dewatering with dynamic compaction is proposed. See Figure 2 for details. The specific implementation plan is as follows:

(1) Upon completion of construction preparations, site clearance, excavation of drainage ditches and assembly and commissioning of the compaction rig, proceed with the positioning and staking out of the dewatering wells. Simultaneously, install water-level observation wells, deep wellpoint dewatering pipes and pore-water-pressure monitoring probes. Once the connection between the well network and the vacuum system has been established, commence dewatering.

(2) Once the water level has reached the required control level and initial pore-water pressure data have been obtained, proceed with the first round of spot compaction and compaction pit operations. Subsequently, provided that the conditions for 'dewatering, monitoring and acceptance' are met, carry out the second and third rounds of spot compaction until both the water level and the dissipation of excess pore-water pressure meet the standards.

(3) Finally, dismantle the temporary dewatering system, whilst retaining the sealed pipe wells to continue dewatering. This is followed by site levelling, dredging, pipe sealing and roller compaction, with third-party testing serving as the final stage for process closure and quality acceptance.

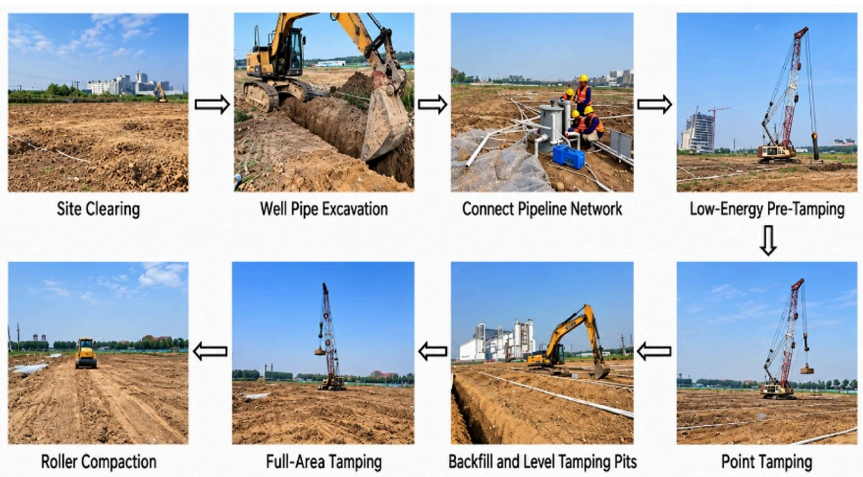

Figure 2. On-site construction process.

2.3. Key Technical Specifications

The combined treatment used an effective vacuum pressure of 70 kPa, a dewatering duration of 30 days and a well depth of 4 m. As listed in Table 3, the row spacing × well spacing of the vacuum wells was 4 m × 5 m. Dynamic compaction comprised six point-compaction passes in which the compaction energy was progressively increased from 1200 to 2200 kJ, followed by a 1000 kJ ironing pass; the point-compaction passes used 4–6 blows per point. The interval between passes was controlled by field monitoring, and the next pass commenced after approximately 80–90% dissipation of excess pore-water pressure. This staged procedure was intended to limit pore-pressure accumulation during repeated compaction.

Table 3. Compaction construction process parameters.

Construction Sequence	Row × Point Spacing of Vacuum Wells (m)	Compaction Energy (kJ)	Tamping Point Spacing (m)	Blows per Point
First pass	4 × 5	1200	4 × 8	4–6
Second pass	4 × 5	1400	4 × 8	4–6
Third pass	4 × 5	1600	4 × 8	4–6
Fourth pass	4 × 5	1800	4 × 8	4–6
Fifth pass	4 × 5	2000	4 × 8	4–6
Sixth pass	4 × 5	2200	4 × 8	4–6
Seventh pass	Ironing compaction	1000	1/4 overlap	1–2

2.4. Field Monitoring and Archived Settlement Dataset

Post-construction settlement prediction in Section 4 is based on the archived settlement series listed in Table 4. The series contains 12 observations from Day 30 to Day 360 at a constant interval of 30 days. In the revised analysis, Day 360 is treated as the last available observation rather than proof that consolidation had ceased. The original monitoring database stored calculated elevation differences to 0.01 mm, while the stated accuracy of the Class IV precision-levelling measurements is ±1 mm. The additional decimal places are retained only to reproduce the archived calculation dataset and should not be interpreted as field measurement precision.

Table 4. Model parameter settings.

Parameter Name	Symbol	Value	Unit
Pore-water density	ρ_f	1000	kg/m^3
Dynamic viscosity of water	μ	1.002×10^{-3}	Pa·s
Solid grain bulk modulus	K_s	3.6×10^{10}	Pa
Pore fluid bulk modulus	K_f	2.2×10^{9}	Pa

Day 0 was defined as the completion of dynamic compaction and site levelling, marking the start of post-construction settlement monitoring. Surface settlement was monitored manually using settlement plates and precision levelling. The stated levelling accuracy was ±1 mm (Class IV levelling). Fifteen settlement monitoring points were arranged in five representative sections, with three monitoring points in each section. Three permanent benchmarks were established on stable hard ground outside the reinforced area. Closed levelling loops were used between the benchmarks and monitoring points, and a fixed route, fixed instrument and fixed staff were maintained during the observations.

Pore-water pressure was monitored using vibrating-wire piezometers installed at depths of 5, 10 and 15 m to cover the principal compressible strata; the stated pressure-measurement accuracy was ±0.5 kPa. Water-level observation wells were also used for construction control, but the complete groundwater-level time histories were not retained in the archived dataset used in this study. Although the field monitoring layout included 15 settlement points, the archived dataset contains only one complete uninterrupted 360-day settlement series suitable for prediction analysis. The series was therefore selected on the basis of data completeness rather than as a spatial average of the full 200,000 m^2 treatment area.

3. Analysis of Post-Construction Settlement Characteristics in Soft Soil Foundations

3.1. Model Development and Parameter Selection

A two-dimensional plane-strain model was established in COMSOL Multiphysics for the warehouse-area cross-section, which has the highest design bearing-capacity requirement in Table 2. The calculation domain was 20 m wide and approximately 18.32 m deep. The model was used to examine the deformation and pore-pressure response of the treated layered ground under the combined dewatering and compaction scheme.

(1) Model Construction and Parameter Selection

The calculation domain was divided into seven strata consistent with Table 1: plain fill, 2-1 silty clay, mucky clay, clay, mucky silty clay, silt and sand intercalated with silty clay, and 3-1 silty clay. Layer interfaces were established from the project investigation data, and the parameter values in Table 1 were assigned to the corresponding strata. Solid mechanics was coupled with Darcy seepage, while the dewatering wells were represented by vertical drainage boundaries at their corresponding locations.

The coupled formulation can be written in standard Biot form as $\nabla\cdot(\sigma' - \alpha pI) + \rho b = 0$ for mechanical equilibrium and $\partial(\alpha\varepsilon\_v + p/M)/\partial t - \nabla\cdot[(k/\mu)\nabla p] = Q$ for fluid mass conservation, where σ' is effective stress, p is pore-water pressure, α is the Biot coefficient, ε_v is volumetric strain, M is the Biot modulus, k is hydraulic conductivity, μ is dynamic viscosity and Q is a fluid source/sink term. These equations describe the two-way coupling between soil deformation and pore-pressure dissipation used in the numerical interpretation.

(2) Boundary Conditions and Mesh Generation

For the mechanical boundary conditions, the base of the model was fixed, the two vertical sides were roller boundaries restricting horizontal displacement, and the ground surface was free except within the loading zone. Dewatering wells were represented by vertical drainage boundaries. The dynamic-compaction action was represented by a transient load applied to the central surface loading zone. A free triangular mesh was used, with local refinement around the wells and loading zone and a minimum element size of approximately 0.25 m. This refinement was intended to resolve pore-pressure gradients near the drainage boundaries and the shallow deformation response.

The computational mesh contained approximately 10,800 finite elements and 16,200 degrees of freedom. For the representative 1600 kJ dynamic-compaction condition, the transient loading was represented using a 20-t hammer dropped from 8 m with a 2.0 m hammer diameter. The 1600 kJ case was selected as an intermediate representative compaction condition rather than reproducing all construction passes individually. With $v = (2gh)^{0.5}$, an impact velocity of approximately 12.53 m/s is obtained. Using an equivalent impact duration $\Delta t = 0.05$ s and a hammer contact area $A = \pi D^2/4 \approx 3.14$ m^2 gives $p = mv/(A\Delta t) \approx 1.60$ MPa, so the equivalent peak surface pressure was taken as approximately 1600 kPa. In the equivalent-load analysis, the hydraulic conductivity, stiffness and strength parameters listed for each stratum were held constant during each transient calculation; compaction-induced evolution of these material parameters was not updated explicitly.

A free triangular mesh was employed, with local refinement around the drainage wells and dynamic compaction loading zone. The computational mesh contained approximately 10,800 triangular elements and 16,200 degrees of freedom. The average element size was approximately 0.28 m, while the minimum element size reached approximately 0.25 m in the refined regions. The mesh quality ranged from 0.75 to 0.85, with an overall mesh qualification rate of approximately 98%. This mesh configuration was considered adequate for resolving the coupled deformation and pore-pressure dissipation processes in the Biot consolidation framework. The numerical simulation results are shown in the Figure 3 below.

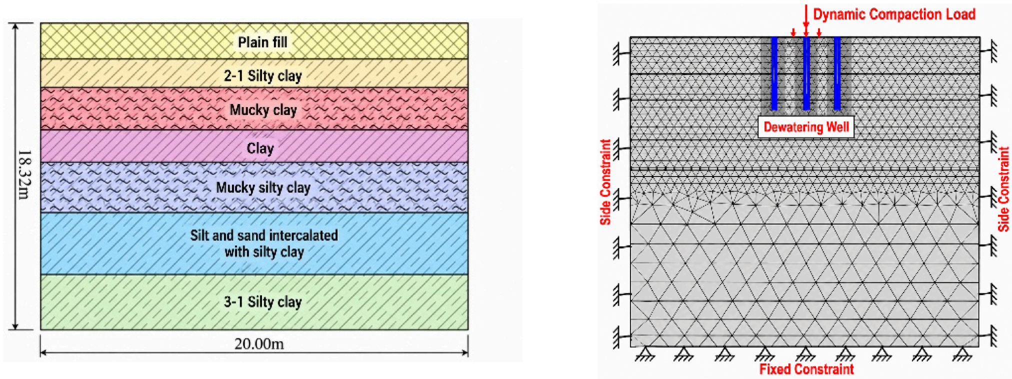

(**a**) Soil layer classification (**b**) Mesh generation and boundary conditions

Figure 3. Geometry, stratigraphy, mesh and boundary conditions of the numerical model.

3.2. Analysis of Numerical Results

(1) Analysis of ground settlement characteristics

The cumulative settlement and the signed vertical settlement rate at the centre point of the ground surface under the combined treatment are shown in Figures 4a and 4b, respectively.

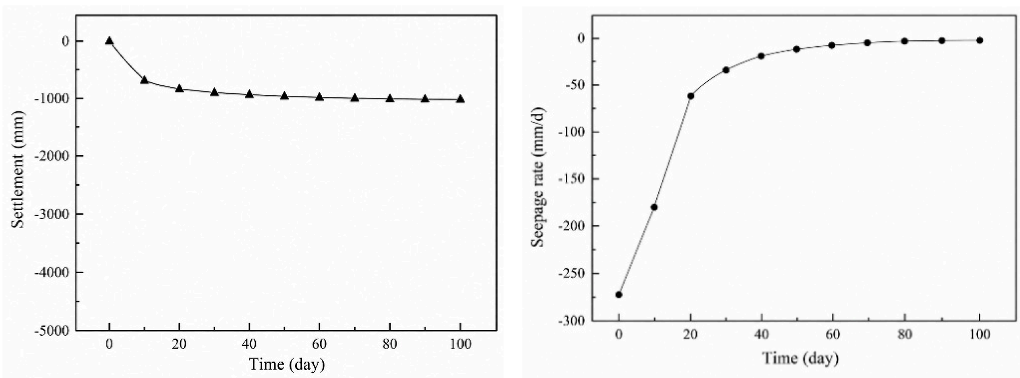

(**a**) Settlement versus time curve (**b**) Signed settlement rate versus time curve

Figure 4. Numerical settlement response at the ground surface.

Figure 4a shows rapid settlement during the early stage followed by progressive convergence, with the simulated cumulative settlement approaching approximately 100 mm by Day 100. This short-term numerical response is not directly equated with the 300–400 mm post-construction control values in Table 2 because the loading stages and time definitions are different. In Figure 4b, downward movement is plotted with a negative sign; therefore, the rise in the signed rate from approximately −28 toward 0 mm/d represents a decrease in the magnitude of the settlement rate as the ground approaches a more stable state. This trend is consistent with progressive consolidation and pore-pressure dissipation in treated soft ground [16,17].

Representative COMSOL settlement outputs were 92.8 mm at Day 30, 105.2 mm at Day 90, 108.3 mm at Day 180 and 108.8 mm at Day 360. The corresponding measured settlements in Table 4 are 92.84, 105.21, 108.33 and 108.84 mm, respectively. For these four matched time points, the mean absolute error (MAE) was 0.030 mm and the root-mean-square error (RMSE) was 0.032 mm. Figure 5 shows the direct comparison between the measured settlement history and the available COMSOL outputs. Because the stated levelling accuracy is ±1 mm, this agreement is interpreted as consistency within the measurement accuracy rather than as sub-millimetre validation precision.

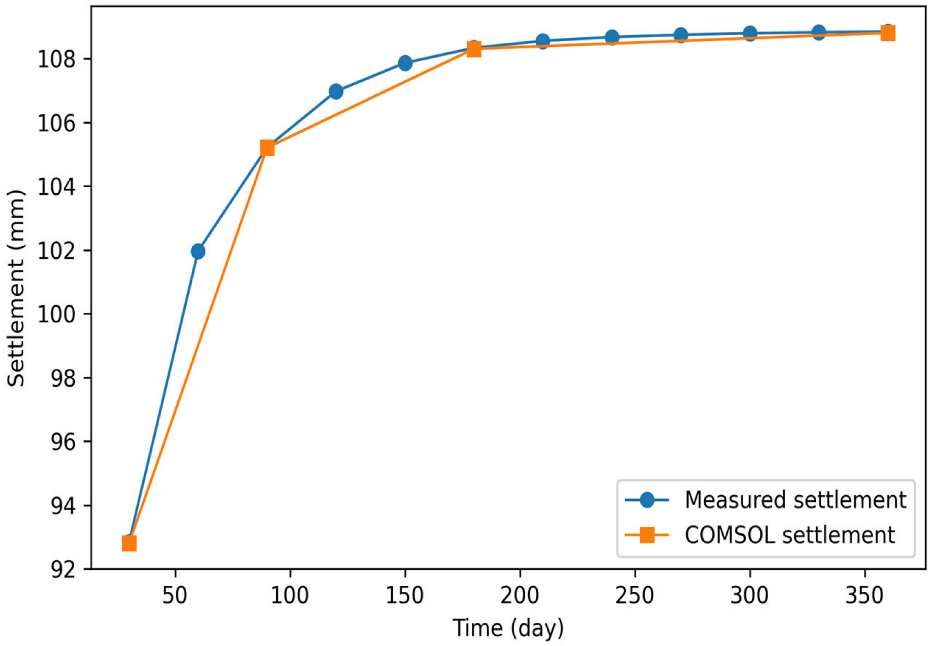

Figure 5. Comparison between measured and COMSOL settlement at selected times.

(2) Pore-Water Pressure Analysis

The Day-10 numerical result was selected to illustrate the spatial distribution of excess pore-water pressure, as shown in Figure 6. The colour scale ranges from 0 to 160 kPa. The plotted field indicates a localised band of residual excess pore-water pressure of roughly 100 kPa near a depth of about 10 m, whereas most of the model domain is substantially lower. This contour is a spatial snapshot and should not by itself be interpreted as validation of the time-dependent dissipation process.

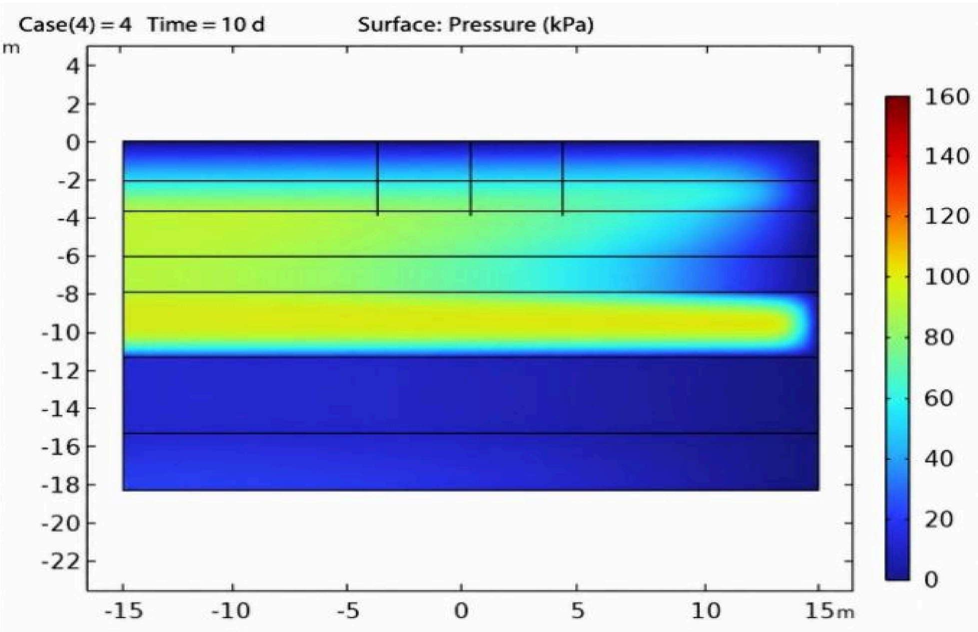

Figure 6. Excess pore-water pressure distribution at Day 10.

As shown in Figure 6, the Day 10 pressure field does not contain an isolated zone approaching the upper colour-scale limit of 160 kPa; instead, the remaining higher-pressure region is spatially localised and transitions gradually into lower-pressure zones. The pattern is consistent with drainage through the imposed well boundaries and redistribution following dynamic compaction. Nevertheless, measured pore-pressure histories are required before the model can be claimed to reproduce the actual dissipation process quantitatively [31].

Taken together, the numerical outputs provide a mechanism-level description of rapid early deformation followed by convergence and of a spatially localised residual pore-pressure field. The matched settlement comparison at Days 30, 90, 180 and 360 provides a limited numerical-to-field check of the deformation response. However, raw pore-pressure and groundwater time histories are not available for direct hydraulic validation; therefore, the pore-pressure dissipation mechanism remains supported primarily by the numerical results. The COMSOL analysis is used to interpret the deformation and pore-pressure mechanisms of the combined treatment, whereas the Asaoka, hyperbolic and exponential methods in Section 4 are calibrated independently from the field settlement observations. Numerical-model outputs are not used as input data for the empirical settlement predictions.

4. Post-Construction Settlement Prediction

4.1. Prediction Formulations and Calibration Protocol

Three established monitoring-based methods were evaluated: the Asaoka method [32], the hyperbolic method [33] and the exponential curve method [34]. The exponential formulation is associated with Terzaghi-type one-dimensional consolidation behaviour. Table 5 contains 12 settlement observations at equal 30-day intervals from Day 30 to Day 360. To avoid information leakage, independent predictive validation used three calibration windows ending at Days 180, 240 and 300; all subsequent observations were withheld from parameter estimation and used only for evaluation. Each method was refitted within each calibration window, and the withheld predictions were assessed using mean absolute error (MAE) and root-mean-square error (RMSE).

Table 5. Archived field settlement series.

Time (day)	**30**	**60**	**90**	**120**	**150**	**180**
Settlement (mm)	92.84	101.96	105.21	106.97	107.86	108.33
Time (day)	**210**	**240**	**270**	**300**	**330**	**360**
Settlement (mm)	108.55	108.67	108.74	108.79	108.82	108.84

Tables 6–8 retain the full-series parameterisation to illustrate the calculation forms used by the three methods. These full-series fits are descriptive only and are not used as independent evidence of predictive accuracy; the actual predictive assessment is reported in Section 4.2 using withheld observations.

(1) Asaoka method prediction

The Asaoka method uses settlement observations at equal time intervals and fits $S_i = \beta_0 + \beta_1 S_{i-1}$. For each calibration window in the revised validation, paired observations from Day 90 onward were used for regression to reduce the influence of the first two early-stage pairs, consistent with the original treatment of the dataset. Future settlements were generated recursively at 30-day steps using only the fitted coefficients and the last observed value within the calibration window. The corresponding asymptotic settlement is $S_\infty = \beta_0/(1 - \beta_1)$.

Table 6. Paired settlement observations for the illustrative Asaoka fit.

i	S_{i-1} (mm)	S_i (mm)	Coordinates (S_{i-1}, S_i)
1	0	92.84	(0, 92.84)
2	92.84	101.96	(92.84, 101.96)
3	101.96	105.21	(101.96, 105.21)
4	105.21	106.97	(105.21, 106.97)
5	106.97	107.86	(106.97, 107.86)
6	107.86	108.33	(107.86, 108.33)
7	108.33	108.55	(108.33, 108.55)
8	108.55	108.67	(108.55, 108.67)
9	108.67	108.74	(108.67, 108.74)
10	108.74	108.79	(108.74, 108.79)
11	108.79	108.82	(108.79, 108.82)
12	108.82	108.84	(108.82, 108.84)

Table 7. Hyperbolic-model parameter transformation.

Time t (day)	Actual Settlement S (mm)	$x = t - t_0$	$S - S_0$	$y = x/(S - S_0)$
30	92.84	0	0	-
60	101.96	30	9.12	3.289
90	105.21	60	12.37	4.850
120	106.97	90	14.13	6.369
150	107.86	120	15.02	7.989
180	108.33	150	15.49	9.684
210	108.55	180	15.71	11.458
240	108.67	210	15.83	13.266
270	108.74	240	15.90	15.094
300	108.79	270	15.95	16.928
330	108.82	300	15.98	18.773
360	108.84	330	16.00	20.625

Table 8. Full-series illustrative exponential-curve parameters.

Time t (day)	*Actual Settlement S* (*mm*)	S/S_∞	$1 - S/S_\infty$	$y = \ln(1 - S/S_\infty)$
30	92.84	0.8530	0.1472	−1.9174
60	101.96	0.9368	0.0632	−2.7615
90	105.21	0.9667	0.0333	−3.4012
120	106.97	0.9828	0.0172	−4.0650
150	107.86	0.9910	0.0090	−4.7121
180	108.33	0.9953	0.0047	−5.3671
210	108.55	0.9974	0.0026	−5.9347
240	108.67	0.9985	0.0015	−6.4737
270	108.74	0.9991	0.0009	−7.0126
300	108.79	0.9996	0.0004	−7.7264
330	108.82	0.9998	0.0002	−8.7072

The regression coefficient β:

$$\beta = \frac{n\sum S_{i-1} \cdot S_i - \sum S_{i-1} \cdot \sum S_i}{n\sum S_{i-1}^2 - \left(\sum S_{i-1}\right)^2} \approx 0.5248 \quad (1)$$

Intercept: β_0:

$$\beta_0 = \frac{\sum S_i - \beta \cdot \sum S_{i-1}}{n} \approx 51.715 \quad (2)$$

The fitted straight line:

$$S_i = 51.715 + 0.5248S_{i-1} \tag{3}$$

In summary, the results calculated using the formula for asymptotic settlement are as follows:

$$S_\infty = \frac{\beta_0}{1-\beta} = \frac{51.715}{1-0.5248} \approx 108.837 \text{ mm} \tag{4}$$

(2) The hyperbolic method:

The first observation was used as the starting point, $t_0 = 30$ d and $S_0 = 92.84$ mm. Let $x = t - t_0$ and $y = x/(S - S_0)$. Linear regression of $y = a + bx$ gives the hyperbolic prediction $S(t) = S_0 + (t - t_0)/[a + b(t - t_0)]$, and the asymptotic settlement is $S_\infty = S_0 + 1/b$. For the out-of-sample tests, a and b were estimated only from observations within the relevant calibration window. The data is presented in Table 7 below.

Substituting the intercept a and the slope b into the formula gives:

$$b = \frac{n\sum xy - \sum x \sum y}{n\sum x^2 - \left(\sum x\right)^2} \approx 0.0581 \tag{5}$$

$$a = \frac{\sum y - b\sum x}{n} \approx 1.2022 \tag{6}$$

The regression equation is therefore:

$$y = 1.2022 + 0.0581x \tag{7}$$

Hyperbolic forecasting model:

$$S_t = 92.84 + \frac{t-30}{1.2022 + 0.0581(t-30)} \tag{8}$$

The asymptotic settlement:

$$S_\infty = S_0 + \frac{1}{b} \approx 110.042 \text{ mm} \tag{9}$$

(3) The exponential curve method

The exponential model is written as $S(t) = S_\infty[1 - \alpha^{-\beta t}]$. For the full-series illustration, the transformation y = ln $[1 - S(t)/S_\infty] = \ln \alpha - \beta t$ may be used once S_∞ is specified. For the independent validation in this revision, S_∞, α and β were estimated by nonlinear least squares using only the observations inside each calibration window, so the withheld observations did not enter parameter estimation.

The previously reported micrometre-scale difference between a model estimate and the Day-360 observation is not treated as evidence of measurement accuracy. Table 5 reports the settlement series to 0.01 mm, whereas the stated accuracy of the Class IV precision-levelling measurements is ±1 mm. Consequently, micrometre- or sub-millimetre-scale differences between model estimates and measured values are not interpreted as direct evidence of measurement accuracy. Day 360 is therefore used as the last reference observation, not as proof of the true final settlement.

The full-series illustrative parameter values are summarised in Table 8.

Linear regression coefficients:

$$b = \frac{n\sum ty - \sum t \sum y}{n\sum t^2 - \left(\sum t\right)^2} = -0.02142 \tag{10}$$

$$a = \frac{\sum y - b\sum t}{n} = -1.42447 \quad (11)$$

$$\beta = -b = 0.02142\ \alpha = e^{a} = e^{-1.42447} = 0.24064 \quad (12)$$

The predictive model is therefore as follows:

$$S(t) = 108.838 \times (1 - 0.24064 \times e^{-0.02142t}) \quad (13)$$

where t is the number of observation days.

The predicted asymptotic settlement is:

$$S_{\infty} = 108.838 \times (1 - 0.24064 \times e^{-0.02142\times 360}) \approx 108.826\ \text{mm} \quad (14)$$

4.2. Out-of-Sample Validation Results

Following the calibration protocol in Section 4.1, Table 9 summarises the RMSE and MAE calculated only from observations that were withheld from model fitting. Figure 7 retains the complete 360-day curves for descriptive visual comparison, but it is not used as the independent validation criterion.

Table 9. Out-of-sample prediction errors (RMSE/MAE, mm).

Calibration Period	Asaoka	Hyperbolic	Exponential
Day 30–180	0.04/0.04	0.87/0.82	0.39/0.38
Day 30–240	0.01/0.01	0.56/0.54	0.14/0.14
Day 30–300	0.02/0.02	0.35/0.34	0.05/0.05

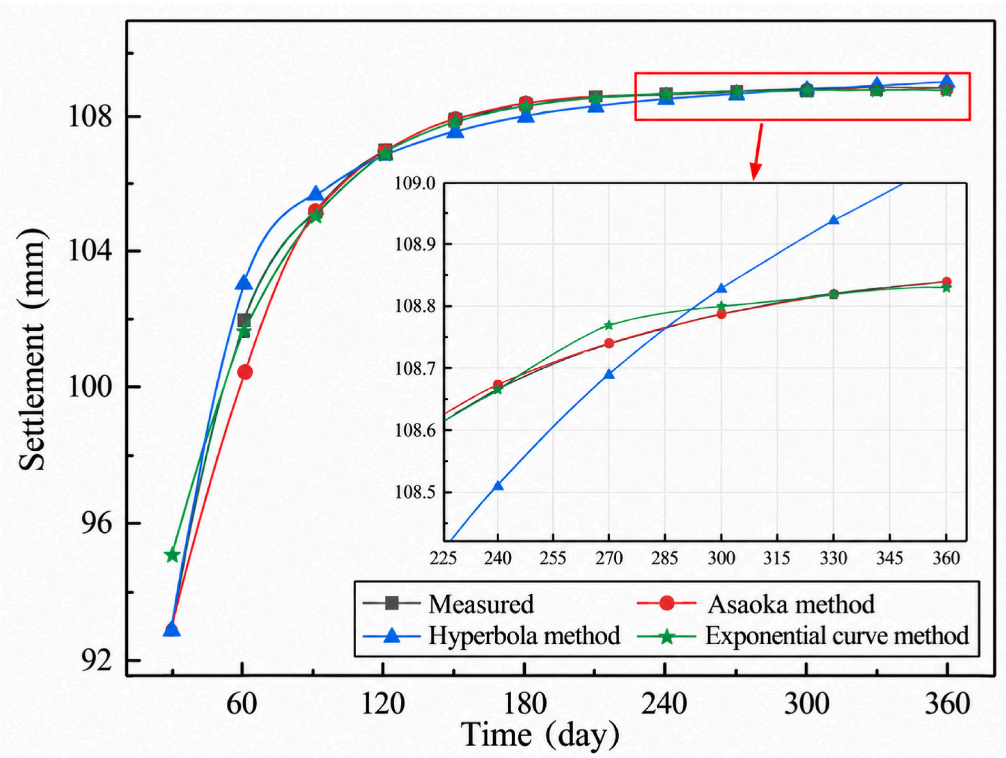

Figure 7. Descriptive full-series fitting curves for the three methods.

For calibration periods ending at Days 180, 240 and 300, the Asaoka method produced RMSE values of 0.04, 0.01 and 0.02 mm, respectively; the corresponding values were 0.87, 0.56 and 0.35 mm for the hyperbolic method and 0.39, 0.14 and 0.05 mm for the exponential method. Averaged over the three validation windows, the RMSE values were 0.02 mm for Asaoka, 0.59 mm for the hyperbolic method and 0.19 mm for the exponential method. These errors are based only on observations that were not used in fitting.

The corresponding Day-360 predictions illustrate the same ranking. With calibration ending at Days 180, 240 and 300, the Asaoka predictions for Day 360 were 108.86, 108.82 and 108.82 mm; the exponential predictions were 108.38, 108.67 and 108.79 mm; and the hyperbolic predictions were 110.05, 109.55 and 109.23 mm. The measured value at Day 360 was 108.84 mm. Because the monitoring series is reported to 0.01 mm and the stated levelling accuracy is ±1 mm, sub-millimetre differences are not over-interpreted as measurement-level accuracy.

The hyperbolic method shows a systematic tendency to overpredict the later observations for this dataset. This behaviour is consistent with its continued extrapolation of the earlier settlement trend when the measured series is already entering a pronounced convergence stage. The reduction in hyperbolic RMSE as the calibration period extends from Day 180 to Day 300 also confirms that the method is sensitive to the selected fitting period.

The exponential method improves substantially as later observations are included in calibration, with RMSE decreasing from 0.39 mm to 0.05 mm. Its remaining early-window underprediction indicates that a single exponential form has difficulty reproducing the rapid transition from early settlement to the very flat late-stage response when only shorter monitoring histories are available.

For this single settlement series, the Asaoka method gives the lowest numerical withheld-data errors across all three calibration windows. However, the RMSE values for both the Asaoka and exponential methods are smaller than the stated ±1 mm levelling accuracy. The present dataset therefore supports only a numerical ranking of the three fitted methods and does not demonstrate a statistically or physically significant superiority of the Asaoka method.

4.3. Discussion and Limitations

The numerical results and the field settlement series are consistent with a treatment response characterised by rapid early deformation followed by a marked reduction in settlement rate. However, the present dataset does not contain a controlled comparison against conventional preloading, vacuum preloading alone or dynamic compaction alone. Likewise, no verified cost, construction-duration, energy-use, material-consumption, carbon-emission or life-cycle dataset is available. The revised manuscript therefore does not claim quantified sustainability, low-carbon or cost superiority for the combined method.

From an engineering perspective, conventional surcharge preloading provides a comparatively simple and controllable loading path but generally requires a longer consolidation period [5,6]. Vacuum preloading can accelerate drainage without a large surface surcharge, although its efficiency depends on vacuum transfer and drainage continuity [7,8]. Dynamic compaction offers rapid densification, but in saturated low-permeability soft soil it may generate substantial excess pore-water pressure if drainage is insufficient [10–13]. The combined scheme used in this project couples dewatering with staged compaction so that drainage is improved before and between impact passes. Because the present study does not include a controlled side-by-side comparison, these differences are discussed qualitatively and are not interpreted as quantified proof of cost, duration, energy or sustainability superiority.

The study is further limited by its single-site design, the absence of an archived three-level mesh/domain sensitivity study, the use of one representative 360-day settlement sequence for prediction despite the wider 15-point monitoring layout, the lack of the complete multi-location settlement time series in the archived dataset, and the absence of raw pore-pressure/groundwater histories for independent hydraulic validation. The

360-day observation should not be equated automatically with the true final settlement, especially for a deep soft-soil deposit. Additional sites, longer monitoring, complete multi-location datasets and direct numerical-to-field hydraulic validation are required before the conclusions can be generalised.

5. Conclusions

(1) The coupled COMSOL model produces a rapid early deformation response followed by convergence, with representative simulated settlements of 92.8, 105.2, 108.3 and 108.8 mm at Days 30, 90, 180 and 360, respectively. The corresponding measured settlements were 92.84, 105.21, 108.33 and 108.84 mm, giving an MAE of 0.030 mm and an RMSE of 0.032 mm for these four matched time points. This numerical agreement is within the stated ±1 mm levelling accuracy and is not interpreted as sub-millimetre measurement precision. The Day-10 excess pore-water-pressure field retains a localised zone of roughly 100 kPa while most of the model domain is lower; raw pore-pressure histories remain unavailable for independent hydraulic validation.

(2) The archived field dataset contains 12 settlement observations at 30-day intervals over 360 days. Independent tests using calibration periods ending at Days 180, 240 and 300 give mean RMSE values of 0.02 mm for the Asaoka method, 0.19 mm for the exponential method and 0.59 mm for the hyperbolic method. The Day-360 settlement of 108.84 mm is used as the last reference observation rather than as a proven final settlement.

(3) Among the three evaluated methods, Asaoka consistently gives the lowest numerical withheld-data errors for this project. Because the differences between the Asaoka and exponential predictions are smaller than the stated ±1 mm levelling accuracy, the present dataset does not establish statistically or physically significant superiority. The recommendation is therefore restricted to a numerical ranking for the investigated monitoring series. Broader conclusions require independent projects, longer-term observations, documented measurement uncertainty, complete multi-location datasets, mesh/domain sensitivity checks and direct validation of the numerical model against measured settlement and pore-water-pressure histories.

Author Contributions: Conceptualization, W.Y. and C.Z.; methodology, J.M.; software, J.M.; validation, Z.W. and Y.X.; writing—original draft preparation, J.O.; writing—review and editing, J.O.; visualization, W.Y.; supervision, C.Z.; All authors have read and agreed to the published version of the manuscript.

Funding: This research received no external funding.

Data Availability Statement: The original contributions presented in this study are included in the article. Further inquiries can be directed to the corresponding author.

Conflicts of Interest: Author Wenkai Yang, Author Zhu Wang and Author Ye Xie were employed by the company Hunan Province Navigation Engineering Co., Ltd., Changsha, China. The remaining authors declare that the research was conducted in the absence of any commercial or financial relationships that could be construed as a potential conflict of interest.

References

1. Wei, F. Research progress of soft soil foundation treatment technology. *Ind. Constr.* **2023**, *53*, 445–447.
2. Jia, Z. Application of soft soil foundation treatment technology in geotechnical engineering. *Value Eng.* **2018**, *37*, 231–232. [CrossRef]
3. Zhao, S.; Yang, Q. Comparison and selection of soft soil characteristics and foundation treatment schemes in Yantian Gangdong operation area. *Water Transp. Eng.* **2025**, 145–151+181.

4. Zhao, Y. Research on soft soil foundation treatment technology for water conservancy projects. *Heilongjiang Water Conserv. Sci. Technol.* **2020**, *48*, 164–166.
5. Zhu, J. Research on the Mechanism and Process of Vacuum Combined Stacking Preload Reinforcement of Soft Foundation. Ph.D. Thesis, Zhejiang University, Hangzhou, China, 2004.
6. Liu, Y.; Yang, W.; You, S. Application of drainage plate stacking preload method in soft foundation treatment of water conservancy projects. *Hydropower Stn. Des.* **2025**, *41*, 42–45.
7. Wang, Y. Reinforcement Characteristics and Numerical Simulation of Foundation Treated by Vacuum Preload. Ph.D. Thesis, Tongji University, Shanghai, China, 2007. [CrossRef]
8. Lv, G.; Ge, J.; Xiao, H. Treatment of coastal soft foundation with cement-soil mixing pile. *J. Shandong Univ. (Eng. Sci.)* **2020**, *50*, 73–81. [CrossRef]
9. Zeng, H.; Zhao, L.; Zhang, J. Experimental study on indoor model of engineering performance of coastal soft foundation deep cement mixing piles. *West. Transp. Sci. Technol.* **2020**, *5*, 15–19. [CrossRef]
10. Meng, Q.; Wang, R. Dynamic response analysis of layered soft foundation treated by strong compaction method. *Rock Soil Mech.* **2006**, *27*, 23–28. [CrossRef]
11. He, L.; Liao, X. Application of strong compaction cushion method in subgrade treatment of soft soil in seaport. *Water Transp. Eng.* **2023**, 185–190.
12. Li, G.; Cai, Z. Engineering application of strong compaction-precipitation combined reinforcement method in blowing fill area. *J. Chang. Univ.* **2015**, *29*, 40–42. [CrossRef]
13. Song, X.; Wang, H.; Zhang, H.; Miao, H.; Liu, X. Field experimental study on the treatment of silty soil foundation by vacuum precipitation-low energy strong compaction combined reinforcement method. *Railw. Archit.* **2011**, 87.
14. Gao, W.; Han, L.; Zhao, Y.; Sun, J.; Liu, L. Consolidation analysis of soft ground with air-boosted vacuum preloading considering attenuation of vacuum and boost pressure. *Sci. Rep.* **2025**, *15*, 23161. [CrossRef] [PubMed]
15. Ge, S.; Jiang, W.; Zheng, L.; Xie, X.; Xie, K. Analytical solution of one-dimensional electroosmotic consolidation considering the starting potential gradient under external load with time change. *Trans. Chin. Soc. Geotech. Eng.* **2023**, *45*, 580–589. [CrossRef]
16. Lei, M.; Luo, S.; Chang, J.; Zhang, R.; Kuang, X.; Jiang, J. Fluid–Solid Coupling Numerical Analysis of Pore Water Pressure and Settlement in Vacuum-Preloaded Soft Foundation Based on FLAC3D. *Sustainability* **2023**, *15*, 7841. [CrossRef]
17. Mamat, R.C.; Ramli, A.; Khahro, S.H.; Yusoff, N.I.M. Numerical Simulation and Field Measurement Validation of Road Embankment on Soft Ground Improved by Prefabricated Vertical Drains: A Comparative Study. *Appl. Sci.* **2022**, *12*, 8097. [CrossRef]
18. Pham, Q.D.; Ngo, V.L.; Tran, T.V.; Trinh, M.T. Evaluation of Asaoka and Hyperbolic Methods for Settlement Prediction of Vacuum Preloading Combined with Prefabricated Vertical Drains in Soft Ground Treatment. *J. Eng. Technol. Sci.* **2022**, *54*, 859–872. [CrossRef]
19. Sun, C.; Yu, T.; Li, M.; Wei, H.; Tan, F. Study on settlement prediction of soft ground considering multiple feature parameters based on ISSA-RF model. *Sci. Rep.* **2024**, *14*, 5067. [CrossRef] [PubMed]
20. Gao, Y.; Mo, Z.; Wei, J. Optimization and application of exponential curve method in soft soil foundation settlement prediction. *Transp. Sci. Eng.* **2011**, *27*, 1–5. [CrossRef]
21. Li, B.; Cheng, W.; Xiang, C. Prediction of settlement after large-area stacking preloading treatment of deep soft foundation. *Trans. Chin. Soc. Geotech. Eng.* **2021**, *43*, 162–165.
22. Liu, Z.; Tang, C.; Wen, J.; Wang, S.; Ma, Z. Prediction method and engineering application of deep soft soil subgrade settlement. *Highway* **2022**, *67*, 103–108.
23. Chen, K.; Yao, Y.; Zhu, B. Practical settlement prediction method considering the whole process of consolidation. *Trans. Chin. Soc. Geotech. Eng.* **2024**, *46*, 103–106.
24. Han, S.; Fu, W.; Zhang, J.; Lin, C. Comparative analysis of different settlement prediction models under small load after soft soil foundation construction. *Sino-Foreign Highw.* **2024**, *44*, 1–10.
25. Meng, X.; Zheng, J.; Yang, B. A new method for predicting consolidation settlements of soft ground based on monitoring results. *Arch. Civ. Eng. (Pol. Acad. Sci.)* **2024**, *70*, 403–416. [CrossRef]
26. Yuan, W.; Zhu, R.; Su, Y.; Feng, Q.; Chu, C.; Deng, Y. Settlement prediction method for staged preloading on soft clay ground. *J. Southeast Univ. (Engl. Ed.)* **2024**, *40*, 41–48. [CrossRef]
27. Huang, L.; Qin, W.; Dai, G.-L.; Zhu, M.-X.; Liu, L.-L.; Huang, L.-J.; Yang, S.-P.; Ge, M.-M. Ground settlement prediction for highway subgrades with sparse data using regression Kriging. *Sci. Rep.* **2024**, *14*, 24594. [CrossRef] [PubMed]
28. Ren, Y. Field Observation and Settlement Prediction Study of a Soft Soil Embankment under Rolling Dynamic Compaction. *Appl. Sci.* **2024**, *14*, 6454. [CrossRef]
29. Guan, Y.; Tang, T.; Chen, H.; Li, X. Field test study on vacuum preloaded shallow reinforcement of ultra-soft foundation. *Trans. Chin. Soc. Geotech. Eng.* **2011**, *33*, 97–101.
30. *GB 50007–2011*; Code for Design of Building Foundation. China Architecture and Building Press: Beijing, China, 2011.

31. Zheng, X.; Dong, Z.; Yang, F. Study on variation of pore-water pressure in soil under vacuum combined with surcharge preloading. *Water Transp. Eng.* **2004**, 4–6. [CrossRef]
32. Wang, Z.; Huang, J.; Li, Y. Research on the application of Asaoka method in settlement prediction. *Rock Soil Mech.* **2006**, *27*, 2025–2028+2032. [CrossRef]
33. Tan, T.S.; Inoue, T.; Lee, S.L. Hyperbolic Method for Consolidation Analysis. *J. Geotech. Eng.* **1991**, *117*, 1723–1737. [CrossRef]
34. Zhang, L.; Xue, X. Application of Exponential Curve Method in Foundation Settlement Prediction. *Water Conserv. Sci. Technol. Econ.* **2016**, *2*, 16–17. [CrossRef]

https://doi.org/10.3390/technologies14090590